Materials Advances

ROYAL SOCIETY OF CHEMISTRY

PAPER

View Article Online
View Journal | View Issue

Cite this: *Mater. Adv.*, 2025, 6, 4357

Vitamin A as a simple, dual-role agent for the band bending-induced passivation of perovskite solar cells†

James C. Solano, [a] Itaru Raifuku, *[ab] Hidenori Kawanishi [a] and Yukiharu Uraoka[a]

Vitamin A (vit A), in the form of retinyl acetate, was used as a passivation material owing to its interesting structural properties: the polar acetate group of vitamin A serves as a linking functional group on perovskite surfaces inducing band-bending, and the non-polar alkyl chain with a π-conjugation system facilitates charge extraction. In this study, solutions of retinyl acetate dissolved in chlorobenzene with varying concentrations were spin-coated on an annealed perovskite film. An improvement of power conversion efficiency (PCE) from 16.3% (control) to 17.6% was observed on the device passivated with a vit A concentration of 2 mg mL^{-1}. The improvement in the overall performance can be attributed to the increase in the fill factor. X-ray photoelectron spectroscopy (XPS) confirmed the interaction between the perovskite surface and vitamin A molecules. Further XPS depth profile analysis revealed a Fermi level shift on the passivated surface relative to the bulk, exhibiting a stronger p-type behavior on the surface compared to the control sample. This resulted in a band bending, driving a more efficient hole-extraction from the perovskite absorber to the spiro-OMeTAD hole transport layer and reducing trap-assisted non-radiative recombination, as supported by time-resolved photoluminescence spectroscopy and ideality factor estimation. Finally, better device stability was observed, with 2 mg mL^{-1} vit A passivated devices maintaining more than 90% of their initial PCE, compared to less than 60% for control devices, for a span of around 800 hours.

Received 3rd March 2025,
Accepted 18th May 2025

DOI: 10.1039/d5ma00192g

rsc.li/materials-advances

Introduction

Perovskite solar cells (PSCs) have emerged as a leading contender for next-generation photovoltaics, offering remarkable efficiency and ease of fabrication. PSC research extends across novel device architectures and fabrication techniques,[1–3] to tailored electron-transport[4–6] and hole-transport[7–9] layers, as well as solvent and compositional engineering of perovskite absorbers[10–12]—advances that collectively continue to increase device performance. However, the practical challenges of interfacial charge recombination, defect states, and long-term stability continue to limit their potential.[13,14] To address these issues, surface passivation has been proven to be a crucial strategy for mitigating defects, enhancing charge transport, and stabilizing perovskite layers.[15,16]

A variety of materials have been explored for passivation purposes, ranging from ions[17–20] and small molecules[21–28] to polymers.[29–35] Among these materials, alkylamines and their halides have emerged as successful passivation agents.[36–45] These molecules are effective in passivating defects on perovskite surfaces, enhancing device stability and efficiency. However, their alkyl chains can sometimes hinder charge transport by increasing the insulating barrier, which reduces charge extraction efficiency. A previous report highlighted that by controlling the alkyl-chain length, a balance between surface-dipole induced charge-coulomb repulsive force and quantum tunneling can be achieved, maximizing the charge extraction.[45]

In contrast, recent studies have focused on designing molecules with bifunctionalities, where one moiety passivates undercoordinated Pb ions, while the other improves charge transport.[25,46,47] For example, a recent publication reported a molecule incorporating a phenylammonium iodide unit that reduces defects on the perovskite surface, and a carbazole-triphenylamine unit whose conjugated structure aligns its energy levels with the perovskite, enhancing charge transfer to the hole transport layer. This dual functionality ultimately led to improved device performance and stability.[46]

[a] *Division of Materials Science, Nara Institute of Science and Technology, Nara 630-0192, Japan. E-mail: ra-itaru@ee.aoyama.ac.jp*
[b] *Department of Electrical Engineering and Electronics, College of Science and Engineering, Aoyama Gakuin University, Kanagawa 252-5258, Japan*

† Electronic supplementary information (ESI) available. See DOI: https://doi.org/10.1039/d5ma00192g

This alignment of energy levels is closely related to the phenomenon of band bending at the perovskite surface, which is induced by the passivation agent. Band bending creates an energetic gradient that drives charge carriers toward the transport layers, promoting efficient charge extraction and minimizing recombination. The importance of band bending in passivation strategies was first highlighted in two notable studies, which shifted the focus of passivation research on understanding the mechanisms rather than solely improving the film properties and solar cell performance. These studies provided valuable insights into how passivation agents influence charge carrier dynamics, paving the way for the rational design of passivators that optimize this effect.[33,35]

In this study, we investigate a similar bifunctional approach using vitamin A (vit A) in the form of retinyl acetate, a simple and readily available molecule. Retinyl acetate features a polar acetate group for anchoring to undercoordinated Pb^{2+} ions on a perovskite surface, effectively reducing defects, and a π-conjugated tail that promotes efficient charge transport. Unlike bifunctional cations built on bulky multi-arm scaffolds, retinyl acetate delivers both defect passivation and efficient hole extraction in a single, simple architecture, while still opening clear avenues for follow-up work—*e.g.*, varying the head-group chemistry (ester → amide → imidazolium) or exploring alternative π-conjugated backbones to fine-tune the dipole moment and conjugation length[48]—all without adding undue synthetic complexity.

While studying the effects of retinyl acetate on perovskite solar cells, we observed band bending on the perovskite surface, mirroring the findings of earlier studies, and providing insights into its dual role in defect passivation and charge carrier dynamics. This study highlights the potential of small, readily available molecule like retinyl acetate to offer practical solutions for improving both the efficiency and stability of PSCs.

Results and discussion

A strategy to passivate a perovskite surface is proposed herein where a simple molecule with interesting chemical structure, vitamin A (vit A) in the form of retinyl acetate, is used to influence the band structure and charge carrier dynamics between the perovskite and the hole transport layer. As schematically shown in Fig. 1a, vit A is hypothesized to reside on the perovskite surface with the acetate functional group serving as the anchoring site by electrostatically interacting with undercoordinated Pb^{2+} ions. X-ray photoelectron spectroscopy (XPS) analysis provided evidence for these interactions by showing a shift in the binding energy of Pb 4f signals to lower energy values as depicted in Fig. 1b. For the control samples, Pb signals appeared at 137.6 eV and 142.5 eV for $4f_{7/2}$ and $4f_{5/2}$, respectively. Upon the addition of vit A, these signals were red-shifted to 137.3 and 142.2 eV, indicating an increase in electron density due to the electron donation effect of vit A. Interestingly, the metallic Pb signal which was observed for pristine samples, was absent for passivated samples. This suggests that vit A acts as a protective layer, preventing the formation of metallic Pb, which is known to accelerate the degradation of perovskite materials.[49] Further analysis using X-ray diffraction (XRD) patterns (Fig. S1, ESI†) showed no significant change in the crystal structure of the perovskite, indicating that vitamin A primarily functions as a surface passivation agent without intercalating into the perovskite crystal lattice. Moreover, the optical band gap energy, another bulk property, remained unchanged with the addition of vitamin A, as shown in Fig. S2 (ESI†). The absence of measurable changes in the band gap and absorption spectra upon surface treatment aligns well with previously reported literature, where surface-passivating agents similarly exhibited no significant influence on bulk optical characteristics when no chemical modification of the perovskite bulk occurred.[35,39,50] Collectively, these results reinforce our conclusion that vitamin A predominantly resides on the surface, effectively passivating defects without altering the bulk perovskite properties.

The effect of vitamin A surface passivation on the device performance was also evaluated. As shown in Fig. 2a, among devices with a structure FTO/SnO_2/Perovskite/Spiro-OMeTAD/Au, the best-performing device exhibited a power conversion efficiency (PCE) of 17.6% compared to 16.3% of the control device. The influence of varying the concentration of the deposited vit A solution was also investigated. For the concentrations of 1, 2 and

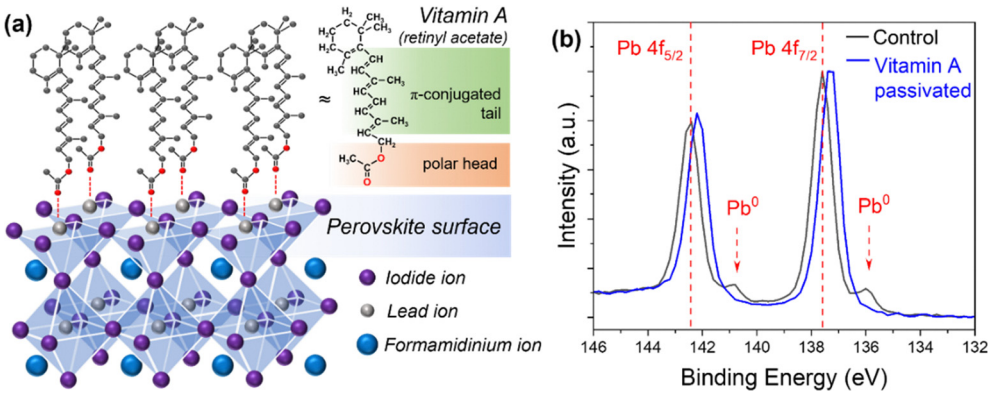

Fig. 1 (a) Schematic illustration of vit A passivation on the perovskite surface. (b) Pb 4f XPS spectra of perovskite films with and without vit A passivation.

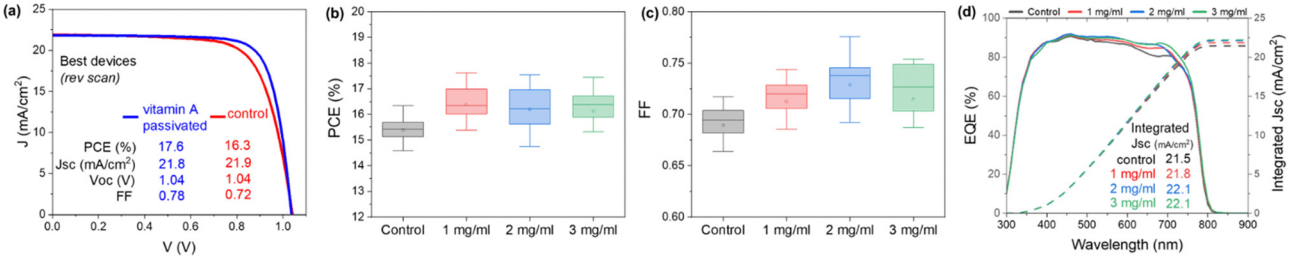

Fig. 2 Photovoltaic performance. *J–V* curves and photovoltaic parameters of the best-performing devices (a) and distribution of PCE (b) and FF (c) of control and passivated devices with varying concentrations of vit A. (d) EQE spectra of the devices with their corresponding integrated J_{SC}.

3 mg mL^{-1} used in the experiment, an overall increase in PCE was observed as shown in Fig. 2b. This increase is mainly attributed to the increase in the fill factor (FF) observed both in the best performing devices and the average values, as shown in Fig. 2c. Other photovoltaic parameters are summarized in Fig. S3 (ESI†). The FF increased with vit A concentration, reaching its highest value of 0.78 for 2 mg mL^{-1} compared to 0.72 for the control device. However, at 3 mg mL^{-1}, the FF declined slightly to a maximum value of 0.74. The diminishing improvement in the FF at higher concentrations suggests that increasing the vit A concentration beyond 2 mg mL^{-1} does not further enhance the device performance, potentially due to saturation effects. This concentration-dependent trend will further be discussed in the subsequent characterization studies. The external quantum efficiencies (EQEs) of the passivated samples also exhibited a notable improvement compared to the control samples, as shown in Fig. 2d. The integrated short-circuit current density ($J_{SC,EQE}$) was calculated by convolving the EQE spectrum with the AM 1.5 G photon-flux reference (NREL, 1000 W m^{-2}). The resulting value agrees with the J_{SC} obtained from current density–voltage (*J–V*) measurements within 2%, confirming the reliability of the observed enhancement. Forward and reverse *J–V* scans of the best-performing devices were also evaluated (Fig. S4, ESI†). While efficiency improved with vit A treatment, no significant suppression of the hysteresis was observed. This indicates that the impact of vit A is more likely associated with surface-level charge extraction, rather than with mitigating ionic or interfacial effects commonly associated with hysteresis.[51] The underlying mechanisms are explored in the following characterization studies.

To gain further insight into the observed improvement in the FF and surface charge dynamics, non-radiative recombination and charge-carrier transport were investigated from device ideality factor values, saturation current density, and photoluminescence spectroscopy (PL) measurements. Generally, the improvement of the FF is strongly influenced by the charge transfer and recombination at the surface/interface between the perovskite layer and carrier transport layer.[38] To characterize the charge recombination, ideality factor (n_{id}) values were estimated from dark *J–V* measurements (Fig. S5, ESI†) by employing a method reported in the literature.[52] Typically, n_{id} = 1 indicates a bimolecular radiative recombination like in an ideal diode with minimal defect-related losses, and n_{id} = 2 is associated with unimolecular nonradiative recombination often mediated by trap states within the band gap.[53] The vit A passivated samples showed improved n_{id} values of 1.92 for 2 and 3 mg mL^{-1}, and 1.97 for 1 mg mL^{-1} compared to 2.25 for control samples as shown in Fig. 3a suggesting that vit A reduces the trap-mediated nonradiative recombination. Complementarily, saturation current density (J_0) values were also extracted from the linear region of the ln*J vs. V* curves using the Shockley diode relation[54] (Fig. S6, ESI†). J_0 decreased from 1.69 × 10^{-10} A cm^{-2} for the control device to 2.46 × 10^{-11}, 1.79 × 10^{-11}, and 3.18 × 10^{-11} A cm^{-2} for devices treated with 1, 2, and 3 mg mL^{-1} vitamin A, respectively. The linear fit details are given in Table S1 (ESI†). The reduction confirms that vitamin A effectively suppresses non-radiative recombination at the perovskite/HTL interface, in agreement with the lower ideality factors.

Perovskite/vit A/spiro-OMeTAD films deposited on glass substrates were prepared along with control samples. As shown

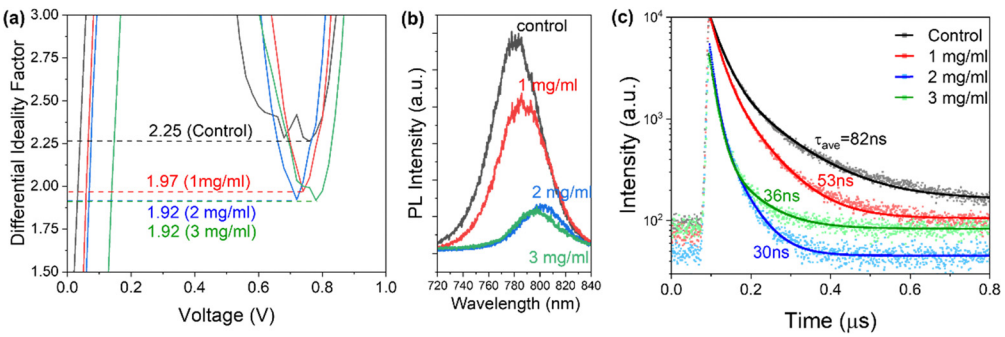

Fig. 3 (a) Differential ideality factor extracted from the device dark *J–V* curves. Steady-state (b) and time-resolved (c) photoluminescence spectra of perovskite/vit A/HTL films deposited on glass with varying concentrations of vit A.

in Fig. 3b, the steady-state PL spectra showed peaks at around 800 nm associated with the emission from the perovskite. A significant reduction of PL intensity was observed when vit A is present as it facilitates effective transport of charge carriers to the HTL.[55] While only around 30% improvement of charge quenching was observed for 1 mg mL^{-1} vit A, it increased to around 80% for 2 and 3 mg mL^{-1}. Interestingly, the PL signal shifted to longer wavelength. This red shift can be ascribed to the quantum confinement due to the increased grain size.[56,57] Fig. S7 (ESI†) shows the scanning electron microscopy images of perovskite films which showed a slight increase in the average grain size, likely due to the post-annealing treatment following the addition of vit A.

Time-resolved PL measurement was also conducted to gain deeper insight into the charge-extraction dynamics at the perovskite/HTL interface in the presence of vit A. As shown in Fig. 3c, TRPL curves of vit A passivated samples exhibit faster decay compared to the control sample. The decay curves were fitted to a biexponential function: $I = I_0 + A_1 \exp(-(t - t_0)/\tau_1) + A_2 \exp(-(t - t_0)/\tau_2)$, where the decay components τ_1 (fast) and τ_2 (slow) corresponding to trap-mediated nonradiative recombination and radiative recombination in the bulk film,[30] respectively, are summarized in Table S2 (ESI†) together with other decay parameters. In the absence of vit A, pristine perovskite films showed relatively long lifetimes with an average of 81.7 ns, while it decreased to 53.1, 29.5, and 35.7 ns for 1, 2, and 3 mg mL^{-1} vit A-passivated samples, respectively. Notably, the amplitude-weighted hole-transfer rate k_{HT} ($= 1/\tau_1$) increases from 3.34×10^7 s^{-1} (control) to 7.69×10^7 s^{-1} at 2 mg mL^{-1} – a ~2.3-fold enhancement – confirming that vit A introduces an efficient decay channel related to the hole transfer from the perovskite to the HTL. However, at 1 mg mL^{-1}, the amount of vit A may be insufficient to fully enhance the charge transport. Meanwhile, increasing to 3 mg mL^{-1} could introduce excessive molecules, potentially hindering the charge transport. From these observations, we conclude that 2 mg mL^{-1} represents the optimal concentration of vit A for achieving a balance between efficient hole transfer and minimal obstruction of charge transport.

To further elucidate the origin of the passivation leading to enhanced charge transport and an overall improvement in the photovoltaic properties, a band diagram (Fig. 4a and Fig. S8a, ESI†) was constructed from the band gap energy (E_g), valence band edge (Fig. S8b, ESI†), and Fermi level (E_F, Fig. S8c–f, ESI†) values obtained from UV-Vis spectroscopy, photoelectron yield spectroscopy (PYS), and XPS measurement, respectively. The measured samples were perovskite films deposited on glass substrates, with and without vit A passivation. Owing to the surface-sensitive nature of PYS and XPS measurements, the constructed band structure reflects the energy levels near the interface between the perovskite and vit A. Notably, the band edges and E_F of the passivated perovskite were shifted to lower energies compared to the pristine perovskite. This downward shift narrows the valence-band offset to the HOMO of spiro-OMeTAD suggesting a significant influence of vit A on the charge carrier dynamics between the perovskite and the HTL,[33,35] consistent with a two-fold increase in k_{HT} extracted from TRPL. The observed lowering of energy levels can also be explained by the dipole nature of vit A, which generates an electric field that reduces the energy levels.[58,59] However, the reduction in the energy level is no longer significant upon increasing the concentration of vit A from 2 to 3 mg mL^{-1}. Depth profile analysis *via* XPS was also performed, revealing how E_F changes with depth in the perovskite layer as shown in Fig. 4b. Consistent with the observation that vit A only binds on the perovskite surface, the energy difference (ΔE) between the valence band edge and Fermi level energy on the surface (0 min sputtering time) for the passivated samples was approximately lower by around 0.5 eV compared to the pristine samples. Upon sputtering to probe deeper layers, ΔE values abruptly increased, plateauing at around 1.5 eV after approximately 1.5 minutes of sputtering for both pristine and passivated samples. Further sputtering did not alter these ΔE values, indicating that the bulk E_F remained unchanged regardless of the presence of vit A. From this result, we verified that the significant electronic changes induced by vit A are confined to the perovskite surface, while the bulk properties remain unaffected. The induced band gradient reflects the localized nature of the vit A's passivation effect, which predominantly alters the electronic states near the surface while maintaining the intrinsic properties of the bulk. The surface-to-bulk gradient introduces band bending, the main driving force for the improved hole transport from the perovskite to the HTL as

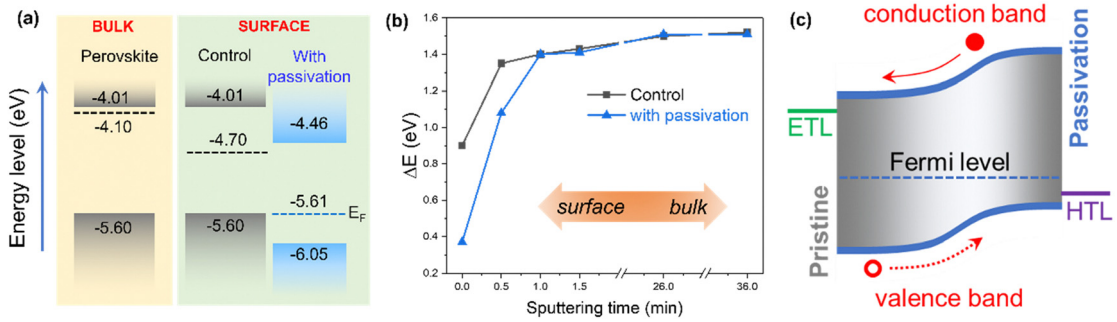

Fig. 4 (a) Energy band diagram of perovskite with and without vit A passivation, where the Fermi level (E_F) is indicated. (b) Depth profile analysis of the Fermi level in perovskite with and without vit A passivation. The concentration of vit A is 2 mg mL^{-1} in (a) and (b). (c) Schematic illustration of the band-bending effect of vit A passivation.

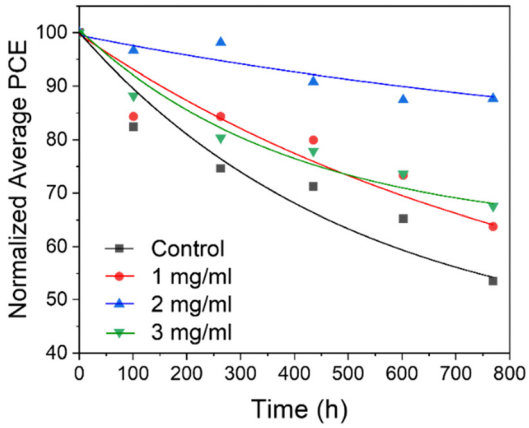

Fig. 5 Stability of perovskite devices with varying concentration of vit A *versus* the control, reported in normalized efficiencies. Storage conditions between measurements were 25 ± 5 °C and 20 ± 10% RH.

schematically shown in Fig. 4c, ultimately contributing to the improved device FF and overall efficiency.

The effect on surface wettability was also examined. Water-contact-angle images (Fig. S9, ESI†) reveal that the untreated perovskite film is hydrophilic, exhibiting an angle of 40.3 ± 1.6°, whereas films treated with 1, 2, and 3 mg mL^{-1} vit A become markedly more hydrophobic, with angles of 68.3 ± 1.1°, 66.0 ± 0.9°, 67.4 ± 2.0°, respectively. The near-identical values indicate saturated surface coverage, with the outward-oriented alkyl chains forming a moisture-repellent barrier.

Finally, stability of the devices was assessed. While all passivated samples exhibited improved efficiency compared to control, devices with 2 mg mL^{-1} vit A demonstrated the best stability among the passivated devices as shown in Fig. 5. The devices were examined for around 800 hours under dark storage conditions at 25 ± 5 °C temperature and 20 ± 10% relative humidity (RH) between measurements. Devices with 2 mg mL^{-1} vit A retained approximately 90% of their initial PCE, whereas those with both 1 mg mL^{-1} and 3 mg mL^{-1} retained approximately 70%. In comparison, the control samples exhibited a significant drop in PCE to less than 60%. These results indicate that vit A significantly improves the device stability with 2 mg mL^{-1} being the optimal concentration. Although both 1 mg mL^{-1} and 2 mg mL^{-1} vit A enhanced the initial PCE, 1 mg mL^{-1} was insufficient to achieve long-term stability. Conversely, at 3 mg mL^{-1}, the excess vit A no longer provided beneficial effects for stability and may have introduced adverse effects.

Conclusions

In conclusion, we have demonstrated that retinyl acetate, a form of vitamin A, acts as an effective surface passivation agent for perovskite solar cells. This passivation reduces the formation of metallic Pb and enhances device stability. It improves the fill factor, primarily by causing band bending on the perovskite surface, which enhances hole extraction. Additionally, non-radiative recombination is suppressed. As a result, devices with vitamin A passivation show better stability and longer operational lifetimes compared to pristine samples.

Experimental

Materials

Fluorine-doped tin oxide (FTO)-coated glass substrates (7 Ω sq^{-1}), tin chloride dihydrate ($SnCl_2{\cdot}2H_2O$), urea, thioglycolic acid (TGA), retinyl acetate, dimethyl formamide (DMF), dimethyl sulfoxide (DMSO), chlorobenzene (CBz), 4-*tert*-butylpyridine (*t*BP), lithium bis(trifluoromethane)sulfonamide (Li-TFSI), and acetonitrile were all purchased from Sigma-Aldrich. Formamidinium iodide (FAI), cesium iodide (CsI), lead iodide (PbI_2), methyl ammonium bromide (MABr), and lead bromide (PbBr) were purchased from Tokyo Chemical Industry (TCI) Co., Ltd. Spiro-OMeTAD was purchased from Advanced Election Technology Co., Ltd. All chemicals were used as received without any purification.

Device fabrication

FTO glass substrates were sequentially cleaned by sonication with a detergent solution, deionized water, isopropyl alcohol, and acetone, followed by chemical bath deposition of the tin oxide (SnO_2) layer by immersing the substrates in an aqueous solution of $SnCl_2{\cdot}2H_2O$ (0.275% w/v), urea (1.25% w/v), HCl (1.25% v/v) and TGA (0.025% v/v), then heating at 90 °C for 4 h. The substrates were then removed and annealed on a hotplate at 200 °C for 1 h. For perovskite deposition, solution of FAI (1.05 M), CsI (0.12 M), PbI_2 (1.17 M), $PbBr_2$ (0.13 M) and MABr (0.13 M) in DMF/DMSO (7 : 3 by volume) was spin-coated (static) on the SnO_2 layer (two-step program: 2000 rpm for 10 s and 5000 rpm for 30 s). The CBz anti-solvent was dripped onto the film surface 10 s before the spinning finishes, followed by annealing of the samples at 100 °C for 1 h to form the perovskite layer. For the passivated samples, solution of retinyl acetate in CBz (with varying concentrations of 1, 2, and 3 mg mL^{-1}) was spin-coated (dynamic) on the perovskite layer at 3000 rpm for 30 s followed by annealing at 60 °C for 10 min. For the hole-transport layer, spiro-OMeTAD solution in CBz (85.8 mg mL^{-1}) with *t*BP (3.6% v/v) and Li-TFSI (0.012 mg mL^{-1}) additives was spin-coated (dynamic) on the perovskite layer at 3000 rpm for 20 s. Finally, an 80 nm gold layer was evaporated on the hole-transport layer to complete the device.

Characterization and measurements

The *J*–*V* and EQE curves were measured using a Bunkoukeiki CEP-2000RP instrument. The measurements were performed under simulated AM 1.5 G spectrum (100 mW cm^{-2}) for devices with an active area of 0.125 cm^2. XPS measurements were carried out using ULVACPHI Versa Probe II with a mono-Al Kα source. For depth profile analysis, a 10kV gas-cluster ion beam (GCIB) was used to sputter the surface. The Au 4f peak (84.0 eV) was used to calibrate the binding energy. Photoluminescence spectra were measured using Coherent Mira900 F with a laser excitation wavelength of 425 nm. Absorption

spectra of the perovskite films were calculated from optical reflectance and transmittance obtained using UV-Vis spectrophotometry (JASCO V-4570). Valence band edges were measured using photoelectron yield spectrometry (Riken Keiki AC-3) under open-air conditions with a measurement range of 4–7 eV. The surface morphology of the films was photographed using a scanning electron microscope (JSM-IT800) with an operating electron detector at 3 kV. Finally, contact angles were recorded with a goniometer (Kyowa Interface 110 Science, DM 300) using 3 μL deionized water droplets.

Author contributions

J. S. conceived the idea, performed the device fabrication and analyses, and wrote the manuscript. I. R. and H. K. assisted in data analyses and writing the manuscript. Y. U. supervised the project. All authors contributed to discussions and to finalizing the manuscript.

Data availability

All data that support the findings of this study are included within the article and ESI† files.

Conflicts of interest

There are no conflicts to declare.

References

1 F. Gao, H. Li, B. Jiao, L. Tan, C. Deng, X. Wang, C. Luo, C. Zhan, E. Debroye, Y. Peng, Y. Yang, C. Yi and Q. Zhao, *Joule*, 2025, **9**, 101787.
2 G. Huang, T. Zhang, W. Lin, L. Qin, S. Z. Kang and X. Li, *Angew. Chem., Int. Ed.*, 2024, **64**, e202420687.
3 C. Wang, Y. Zhao, T. Ma, Y. An, R. He, J. Zhu, C. Chen, S. Ren, F. Fu, D. Zhao and X. Li, *Nat. Energy*, 2022, **7**, 744–753.
4 S. Tian, X. X. Gao, D. Reyes, O. A. Syzgantseva, M. M. Baytemirov, N. Shibayama, H. Kanda, P. A. Schouwink, Z. Fei, L. Zhong, F. F. Tiranito, Y. Fang, P. J. Dyson and M. K. Nazeeruddin, *Small*, 2024, **20**, 2406929.
5 S. Ahmmed, Y. He, M. E. Kayesh, M. A. Karim, K. Matsuishi and A. Islam, *ACS Appl. Mater. Interfaces*, 2024, **16**, 32282–32290.
6 S. Shin, Y. kim, S. Park, Y. H. Bae and J. S. Noh, *Sol. Energy*, 2024, **277**, 112754.
7 X. Zhang, X. Liu, F. F. Tirani, B. Ding, J. Chen, G. Rahim, M. Han, K. Zhang, Y. Zhou, H. Quan, B. Li, W. Du, K. G. Brooks, S. Dai, Z. Fei, A. M. Asiri, P. J. Dyson, M. K. Nazeeruddin and Y. Ding, *Angew. Chem., Int. Ed.*, 2024, **63**, e202320152.
8 A. Zhang, Y. Chen, Y. Xu, H. Wang, X. Zong, Z. Sun, M. Liang and S. Xue, *ACS Appl. Energy Mater.*, 2024, **7**, 11741–11753.
9 K. Manda, V. D. Jadhav, P. Chetti, R. Gundla and S. Pola, *Org. Electron.*, 2025, **136**, 107153.
10 J. Chen, X. Sun, Z. Wang, X. Cui, X. Chen, Z. Li, X. Feng, J. Tang, M. Yang, Z. Yuan, Z. Zhang, S. La, X. Li, S. Dai and M. Cai, *Adv. Funct. Mater.*, 2025, **35**, 2411010.
11 M. Saliba, T. Matsui, J.-Y. Seo, K. Domanski, J.-P. Correa-Baena, M. Khaja, S. M. Zakeeruddin, W. Tress, A. Abate, A. Hagfeldt and M. Grätzel, *Energy Environ. Sci.*, 2016, **9**, 1989–1997.
12 M. J. Kadhim and M. K. A. Mohammed, *Mater. Res. Bull.*, 2023, **158**, 112047.
13 C. M. Wolff, P. Caprioglio, M. Stolterfoht and D. Neher, *Adv. Mater.*, 2019, **31**, 1902762.
14 T. S. Sherkar, C. Momblona, L. Gil-Escrig, J. Ávila, M. Sessolo, H. J. Bolink and L. J. A. Koster, *ACS Energy Lett.*, 2017, **2**, 1214–1222.
15 V. S. Katta, M. Waheed and J. H. Kim, *Solar RRL.*, 2024, **8**, 2300908.
16 S. Akin, N. Arora, S. M. Zakeeruddin, M. Grätzel, R. H. Friend and M. I. Dar, *Adv. Energy Mater.*, 2020, **10**, 1903090.
17 D. Y. Son, S. G. Kim, J. Y. Seo, S. H. Lee, H. Shin, D. Lee and N. G. Park, *J. Am. Chem. Soc.*, 2018, **140**, 1358–1364.
18 C. Bi, X. Zheng, B. Chen, H. Wei and J. Huang, *ACS Energy Lett.*, 2017, **2**, 1400–1406.
19 S. Bag and M. F. Durstock, *ACS Appl. Mater. Interfaces*, 2016, **8**, 5053–5057.
20 Y. Wen, Y.-G. Tang and G.-Q. Yan, *AIP Adv.*, 2018, **8**, 095226.
21 H. Elbohy, H. Suzuki, T. Nishikawa, A. K. K. Kyaw and Y. Hayashi, *ACS Appl. Energy Mater.*, 2024, **7**, 2925–2937.
22 Z. He, M. Li, H. Jia, R. Yu, Y. Zhang, R. Wang, Y. Dong, X. Liu, D. Xu and Z. Tan, *Adv. Mater.*, 2023, **35**, 2304918.
23 R. K. Gupta, R. Garai, B. Sharma, M. A. Afroz, Yukta, S. Choudhary, P. K. Iyer and S. Satapathi, *Energy Fuels*, 2023, **37**, 667–674.
24 R. K. Gupta, R. Garai and P. K. Iyer, *ACS Appl. Energy Mater.*, 2022, **5**, 1571–1579.
25 B. Zhao, X. Yan, T. Zhang, X. Ma, C. Liu, H. Liu, K. Yan, Y. Chen and X. Li, *ACS Appl. Mater. Interfaces*, 2020, **12**, 9300–9306.
26 R. Garai, M. A. Afroz, R. K. Gupta and P. K. Iyer, *Adv. Sustainable Syst.*, 2020, **4**, 2000078.
27 Y. Lin, L. Shen, J. Dai, Y. Deng, Y. Wu, Y. Bai, X. Zheng, J. Wang, Y. Fang, H. Wei, W. Ma, X.-C. Zeng, X. Zhan and J. Huang, *Adv. Mater.*, 2017, **29**, 1604545.
28 A. Q. Alanazi, D. J. Kubicki, D. Prochowicz, E. A. Alharbi, M. E. F. Bouduban, F. Jahanbakhshi, M. Mladenović, J. V. Milić, F. Giordano, D. Ren, A. Y. Alyamani, H. Albrithen, A. Albadri, M. H. Alotaibi, J. E. Moser, S. M. Zakeeruddin, U. Rothlisberger, L. Emsley and M. Grätzel, *J. Am. Chem. Soc.*, 2019, **141**, 17659–17669.
29 Z. Jia, R. Wang, L. Zhu, A. Altujjar, P. Jacoutot, O. M. Alkhudhari, M. Z. Mokhtar, B. F. Spencer, N. W. Hodson, X. Wang, M. Osborne-Richards, A. G. Thomas, T. Hashimoto, M. Faulkner, D. J. Lewis, S. A. Haque, M. S. Islam, J. M. Saunders and B. R. Saunders, *Energy Environ. Sci.*, 2024, **17**, 7221–7233.
30 D.-H. Kang, C. Ma and N.-G. Park, *Antiseptic Povidone-Iodine Heals Grain Boundary of Perovskite Solar Cells*.

31 J. Jiang, X. Lang, Q. Zeng, M. B. Faheem, S. Rong, H. Zhao and Y. Li, *J. Mater. Chem. A*, 2021, **9**, 13220–13230.
32 Y. Chung, K. S. Kim and J. W. Jung, *Int. J. Energy Res.*, 2022, **46**, 6012–6021.
33 H. Kanda, N. Shibayama, M. Abuhelaiqa, S. Paek, R. Kaneko, N. Klipfel, A. A. Sutanto, C. R. Carmona, A. J. Huckaba, H. Kim, C. Momblona, A. M. Asiri and M. K. Nazeeruddin, *J. Mater. Chem. A*, 2020, **8**, 17113–17119.
34 L. Zuo, H. Guo, D. W. Dequilettes, S. Jariwala, N. De Marco, S. Dong, R. Deblock, D. S. Ginger, B. Dunn, M. Wang and Y. Yang, *Polymer-modified halide perovskite films for efficient and stable planar heterojunction solar cells*, 2017.
35 H. Kanda, N. Shibayama, A. J. Huckaba, Y. Lee, S. Paek, N. Klipfel, C. Roldán-Carmona, V. I. E. Queloz, G. Grancini, Y. Zhang, M. Abuhelaiqa, K. T. Cho, M. Li, M. D. Mensi, S. Kinge and M. K. Nazeeruddin, *Energy Environ. Sci.*, 2020, **13**, 1222–1230.
36 S. Rahmany and L. Etgar, *Mater. Adv.*, 2021, **2**, 2617–2625.
37 Y. Zheng, Y. Li, R. Zhuang, X. Wu, C. Tian, A. Sun, C. Chen, Y. Guo, Y. Hua, K. Meng, K. Wu and C. C. Chen, *Energy Environ. Sci.*, 2023, **17**, 1153–1162.
38 W.-Q. Wu, J.-X. Zhong, J.-F. Liao, C. Zhang, Y. Zhou, W. Feng, L. Ding, L. Wang and D.-B. Kuang, *Nano Energy*, 2020, **75**, 104929.
39 L. Zheng, L. Shen, Z. Fang, P. Song, W. Tian, J. Chen, K. Liu, Y. Luo, P. Xu, J. Yang, C. Tian, L. Xie and Z. Wei, *Adv. Energy Mater.*, 2023, **13**, 2301066.
40 S. Zhou, B. M. Gallant, J. Zhang, Y. Shi, J. Smith, J. N. Drysdale, P. Therdkatanyuphong, M. Taddei, D. P. McCarthy, S. Barlow, R. C. Kilbride, A. Dasgupta, A. R. Marshall, J. Wang, D. J. Kubicki, D. S. Ginger, S. R. Marder and H. J. Snaith, *J. Am. Chem. Soc.*, 2024, **146**, 27405–27416.
41 Z. Xu, N. Liu, X. Liu, W. Han, W. W. Xu, J. Zhang, L. Huang, Z. Hu and Y. Zhu, *Chem. Eng. J.*, 2023, **451**, 139047.
42 B. Yang, J. Suo, F. Di Giacomo, S. Olthof, D. Bogachuk, Y. Kim, X. Sun, L. Wagner, F. Fu, S. M. Zakeeruddin, A. Hinsch, M. Gratzel, A. Di Carlo and A. Hagfeldt, *ACS Energy Lett.*, 2021, **6**, 3916–3923.
43 H.-T. Hsu, Y.-M. Kung, S. Venkatesan, H. Teng and Y.-L. Lee, *Solar RRL*, 2023, **7**, 2300122.
44 S. Yang, Y. Wang, P. Liu, Y.-B. Cheng, H. J. Zhao and H. G. Yang, *Nat. Energy*, 2016, **1**, 15016.
45 J. Duan, Y. Wang, X. Yang and Q. Tang, *Angew. Chem.*, 2020, **132**, 4421–4425.
46 S. You, F. T. Eickemeyer, J. Gao, J. H. Yum, X. Zheng, D. Ren, M. Xia, R. Guo, Y. Rong, S. M. Zakeeruddin, K. Sivula, J. Tang, Z. Shen, X. Li and M. Grätzel, *Nat. Energy*, 2023, **8**, 515–525.
47 Y. Wu, H. Zhu, D. Wang, S. Akin, F. T. Eickemeyer, D. Ren, H. Cai and L.-B. Huang, *Solar RRL*, 2022, **6**, 2200115.
48 D. Koseki, C. A. M. Senevirathne, D. Senba, Y. Fujita, J. Lin, M. Zhai, J. Shang, T. B. Raju, S. Ida, M. Watanabe, A. Staykov, H. Segawa, Z. Guo and T. Matsushima, *J. Mater. Chem. A*, 2025, DOI: **10.1039/D5TA00754B**.
49 J. Liang, X. Hu, C. Wang, C. Liang, C. Chen, M. Xiao, J. Li, C. Tao, G. Xing, R. Yu, W. Ke and G. Fang, *Joule*, 2022, **6**, 816–833.
50 M. Chen, Z. Dai, N. Yan, Y. Cao, Y. Yuan, J. Zhang, D. Qi, L. Meng, S. (Frank) Liu and J. Feng, *J. Mater. Chem. C*, 2024, **12**, 10540–10547.
51 S. Tammireddy, M. N. Lintangpradipto, O. Telschow, M. H. Futscher, B. Ehrler, O. M. Bakr, Y. Vaynzof and C. Deibel, *J. Phys. Chem. Lett.*, 2024, **15**, 1363–1372.
52 W. Tress, M. Yavari, K. Domanski, P. Yadav, B. Niesen, J. P. Correa Baena, A. Hagfeldt and M. Graetzel, *Energy Environ. Sci.*, 2018, **11**, 151–165.
53 P. Caprioglio, C. M. Wolff, O. J. Sandberg, A. Armin, B. Rech, S. Albrecht, D. Neher and M. Stolterfoht, *Adv. Energy Mater.*, 2020, **10**, 2000502.
54 M. Cai, N. Ishida, X. Li, X. Yang, T. Noda, Y. Wu, F. Xie, H. Naito, D. Fujita and L. Han, *Joule*, 2018, **2**, 296–306.
55 T. Jiang and W. Fu, *RSC Adv.*, 2018, **8**, 5897–5901.
56 V. Malgras, S. Tominaka, J. W. Ryan, J. Henzie, T. Takei, K. Ohara and Y. Yamauchi, *J. Am. Chem. Soc.*, 2016, **138**, 13874–13881.
57 Q. Zeng, X. Zhang, X. Feng, S. Lu, Z. Chen, X. Yong, S. A. T. Redfern, H. Wei, H. Wang, H. Shen, W. Zhang, W. Zheng, H. Zhang, J. S. Tse and B. Yang, *Adv. Mater.*, 2018, **20**, 1705393.
58 Z. Hu, Z. Zhong, K. Zhang, Z. Hu, C. Song, F. Huang, J. Peng, J. Wang and Y. Cao, *NPG Asia Mater.*, 2017, **9**, e379.
59 Y. Ma, J. Gong, P. Zeng and M. Liu, *Nano-Micro Lett.*, 2023, **15**, 173.